


NANO EXPRESS

Open Access



Terminal Groups-Dependent Near-Field Enhancement Effect of $\text{Ti}_3\text{C}_2\text{T}_x$ Nanosheets

Ying-Ying Yang¹, Wen-Tao Zhou¹, Wei-Long Song¹, Qing-Quan Zhu¹, Hao-Jiang Xiong¹, Yu Zhang¹, Sheng Cheng², Pai-Feng Luo¹ and Ying-Wei Lu^{1,3*} 

Abstract

Both multilayered (ML) and few-layered (FL) $\text{Ti}_3\text{C}_2\text{T}_x$ nanosheets have been prepared through a typical etching and delaminating procedure. Various characterizations confirm that the dominant terminal groups on ML- $\text{Ti}_3\text{C}_2\text{T}_x$ and FL- $\text{Ti}_3\text{C}_2\text{T}_x$ are different, which have been assigned to O-related and hydroxyl groups, respectively. Such deviation of the dominant terminals results in the different physical and chemical performance and eventually makes the nanosheets have different potential applications. In particular, before coupling to Ag nanoparticles, ML- $\text{Ti}_3\text{C}_2\text{T}_x$ can present stronger near-field enhancement effect; however, Ag/FL- $\text{Ti}_3\text{C}_2\text{T}_x$ hybrid structure can confine stronger near-field due to the electron injection, which can be offered by the terminated hydroxyl groups.

Keywords: Multilayered $\text{Ti}_3\text{C}_2\text{T}_x$, Few-layered $\text{Ti}_3\text{C}_2\text{T}_x$, Terminal group, Near-field enhancement, Coupling

Introduction

$\text{Ti}_3\text{C}_2\text{T}_x$, a typical two-dimensional layered transition metal carbide with a graphene-like structure, has attracted great attention due to its wide potential applications in fields of catalysis, energy, and medicine thanks to its unique properties, especially large specific surface area and so on [1–6]. It has been demonstrated that the physical and chemical performance of $\text{Ti}_3\text{C}_2\text{T}_x$ could be determined by its terminal groups, referred as T_x in the formula (usually are $-\text{F}$, $-\text{O}$ and/or $-\text{OH}$), which can be adjusted by choosing different preparation procedures [7, 8]. For example, some experimental results indicate that the hydrophilic hydrophobic equilibrium of $\text{Ti}_3\text{C}_2\text{T}_x$ can be modulated by interacting some agent groups with $-\text{O}$ terminal groups on $\text{Ti}_3\text{C}_2\text{T}_x$ [9], and the Pb adsorption capacity can be improved by connecting with hydroxyl groups on $\text{Ti}_3\text{C}_2\text{T}_x$ [10]. In the meantime, some theoretical works have determined that the attached methoxy groups could improve the stability

of Ti_2C and Ti_3C_2 [11], and O-related terminal groups could enhance the lithium ion storage capacity of various nanosheets [12]. Apart from the multifarious applications by taking advantage of the unique layered structure with certain terminal groups, it is found that $\text{Ti}_3\text{C}_2\text{T}_x$ can present plasmonic performance as well, and the resonance wavelength can be tuned by the terminals and/or thickness [13], indicating that $\text{Ti}_3\text{C}_2\text{T}_x$ could confine electromagnetic field under excitation and eventually can be employed as broadband perfect absorbers [14, 15], Terahertz shielding devices [16], and photonic and/or molecular detectors or sensors [17–19]. However, most of previous works either concerned the etching condition dependent terminal groups [20] or focused on the overall plasmonic performance [21]. Therefore, it is interesting to systematically study the relationship between the terminal groups of $\text{Ti}_3\text{C}_2\text{T}_x$ with different layers and their near-field enhancement effect, since such effect has been widely employed in many optical related fields, such as surface-enhanced Raman scattering detection, due to the strong confined electromagnetic field [22–24].

In this work, in order to simplify the terminal options and avoid using hazardous HF, the mixed etching agent of LiF and HCl has been used to minimize the fluorine

*Correspondence: luyw@hfut.edu.cn

¹ School of Materials Science and Engineering, Hefei University of Technology, Hefei 230009, People's Republic of China
Full list of author information is available at the end of the article

terminals (-F) in the etching process [25]. Furthermore, the procedure of sonication in water has been carried out to delaminate the multilayered $\text{Ti}_3\text{C}_2\text{T}_x$ (ML- $\text{Ti}_3\text{C}_2\text{T}_x$) into few-layered $\text{Ti}_3\text{C}_2\text{T}_x$ (FL- $\text{Ti}_3\text{C}_2\text{T}_x$) without introducing any other reagents. As a result, the obtained $\text{Ti}_3\text{C}_2\text{T}_x$ with different layers in this work will be mainly terminated by either O- or OH-related groups, which make ML- $\text{Ti}_3\text{C}_2\text{T}_x$ or FL- $\text{Ti}_3\text{C}_2\text{T}_x$ nanosheets reveal different physical and chemical properties and eventually present different near-field enhancement performance. In addition, the hybrid structures composed of $\text{Ti}_3\text{C}_2\text{T}_x$ and Ag nanoparticles have been prepared and the corresponding coupling effects have been explored as well. Such exploration regarding terminal dependent plasmonic performance of these $\text{Ti}_3\text{C}_2\text{T}_x$ with different layers and configurations could help people to select suitable $\text{Ti}_3\text{C}_2\text{T}_x$ -based materials in some specific optical fields.

Methods

Preparation of $\text{Ti}_3\text{C}_2\text{T}_x$ Nanosheets

ML- $\text{Ti}_3\text{C}_2\text{T}_x$ was prepared by following a modified previously reported method [26]. The typical etching process started with the preparation of LiF solution by dissolving 1 g of LiF in 20 mL of dilute HCl solution (6 M) with stirring. Subsequently, 1 g of Ti_3AlC_2 powder was slowly added into the above solution, and the etching process was kept at 70 °C for 45 h under stirring. The wet sediment was then washed several times with deionized water until the pH of the suspension liquid was bigger than 6. Afterward, the suspension was collected and named as ML- $\text{Ti}_3\text{C}_2\text{T}_x$. To obtain FL- $\text{Ti}_3\text{C}_2\text{T}_x$, ML- $\text{Ti}_3\text{C}_2\text{T}_x$ was further delaminated by sonication for 2 h in Ar atmosphere and followed by centrifugation at 3500 rpm for 1 h.

Preparation of Ag/ $\text{Ti}_3\text{C}_2\text{T}_x$ Nanocomposites

The synthesis of the hybrid materials was started with the preparation of the mixed solution of AgNO_3 (12.5 mL, 2 mmol/L) and $\text{NaC}_6\text{H}_5\text{O}_7$ (12.5 mL, 4 mmol/L) at room temperature. After rapidly adding PVP solution (25 mL, 0.1 g/mL), $\text{Ti}_3\text{C}_2\text{T}_x$ solution (5 mL, 0.05 mg/mL) was then slowly added into the mixed solution with stirring for 10 min at room temperature. Subsequently, the above-mixed solution was heated up to 70 °C to react for 45 h. After centrifuging, the products were kept in water and named as Ag/ML- $\text{Ti}_3\text{C}_2\text{T}_x$ and Ag/FL- $\text{Ti}_3\text{C}_2\text{T}_x$, respectively, according to the type of $\text{Ti}_3\text{C}_2\text{T}_x$ used in the procedure.

Characterization

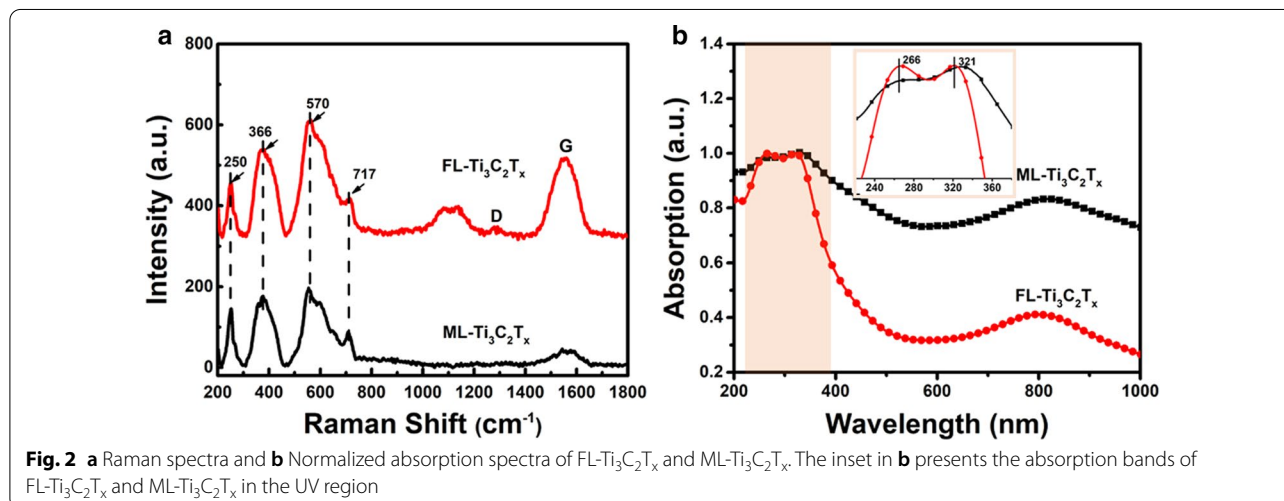
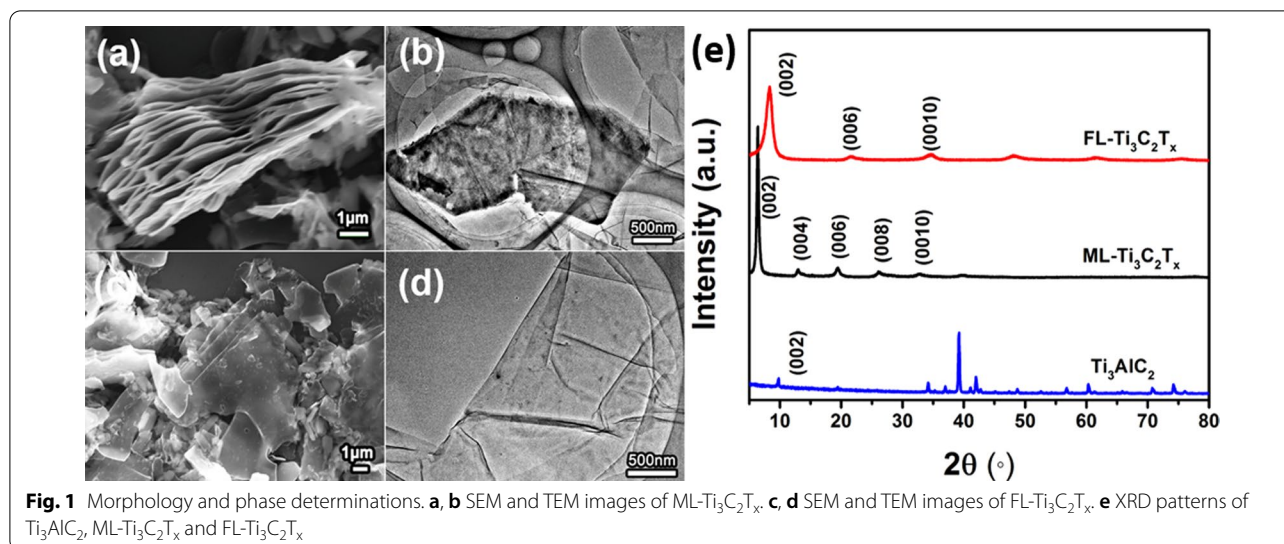
A field emission scanning electron microscope (Carl ZEISS Sigma) and two transmission electron microscopes (JEM-2100F and JEM-1400Flash) have been employed to determine the morphologies of the samples. The X-ray

diffraction (XRD) patterns in the range of $2\theta=5^\circ-80^\circ$ with a step of 0.02° were recorded on a powder diffractometer (X'Pert PRO MPD). Zeta potentials and surface states of ML- $\text{Ti}_3\text{C}_2\text{T}_x$ and FL- $\text{Ti}_3\text{C}_2\text{T}_x$ were measured by a Malvern Zetasizer (Nano-ZS90) and an X-ray photoelectron spectroscopy (XPS, ESCALAB 250Xi), respectively. The absorption and Raman performance of samples were recorded by a UV-Vis spectrophotometer (CARY 5000) and a Raman spectroscopy (LabRAM HR Evolution), respectively. The excitation wavelength of Raman detection was 532 nm, and the laser powers for usual Raman measurements and surface enhanced Raman scattering (SERS) characterizations were 12.5 mW and 0.05 mW, respectively.

Results and Discussion

Both morphologies of ML- $\text{Ti}_3\text{C}_2\text{T}_x$ and FL- $\text{Ti}_3\text{C}_2\text{T}_x$ are shown in Fig. 1a, b and c, d, respectively. It can be seen that FL- $\text{Ti}_3\text{C}_2\text{T}_x$ looks more transparent, indicating that its layer number is much less than ML- $\text{Ti}_3\text{C}_2\text{T}_x$. Figure 1e shows the XRD patterns of all samples. Ti_3AlC_2 and ML- $\text{Ti}_3\text{C}_2\text{T}_x$ show their typical phase features, which agree well with some previous reports [26–28]. It can be readily observed that the intense (002) peak of ML- $\text{Ti}_3\text{C}_2\text{T}_x$ shifts to the lower angle comparing with that of Ti_3AlC_2 , implying the removal of Al atoms from the MAX phase and the expanding along the c axis. Compared with the diffraction peaks of ML- $\text{Ti}_3\text{C}_2\text{T}_x$, both broadened (002) peak and disappeared (004) and (008) peaks of FL- $\text{Ti}_3\text{C}_2\text{T}_x$ determined the successful preparation of the few-layered sample [29]. Moreover, the (002) peak of FL- $\text{Ti}_3\text{C}_2\text{T}_x$ locates at a little higher angle than that of ML- $\text{Ti}_3\text{C}_2\text{T}_x$, indicating that ML- $\text{Ti}_3\text{C}_2\text{T}_x$ and FL- $\text{Ti}_3\text{C}_2\text{T}_x$ should be terminated with different groups, which can be attributed to -O and -OH, respectively, since the as-prepared $\text{Ti}_3\text{C}_2\text{T}_x$ (ML- $\text{Ti}_3\text{C}_2\text{T}_x$) will not be mainly terminated with -F without HF as etching agent and the corresponding c parameters attracted from the XRD patterns agree well with what previous works reported [25, 30].

Figure 2a shows Raman spectra of ML- $\text{Ti}_3\text{C}_2\text{T}_x$ and FL- $\text{Ti}_3\text{C}_2\text{T}_x$. As it can be seen that the Raman signals in the range of 200–800 cm^{-1} for both samples are quite similar. Among them, the peak at 717 cm^{-1} is due to the A_{1g} symmetrical out-of-plane vibration of Ti and C atoms, while the peaks at 244, 366 and 570 cm^{-1} are arising from the in-plane (shear) modes of Ti, C and surface terminal groups, respectively [31, 32]. As for the Raman signals ranging from 800 to 1800 cm^{-1} , comparing with ML- $\text{Ti}_3\text{C}_2\text{T}_x$, FL- $\text{Ti}_3\text{C}_2\text{T}_x$ not only shows stronger Raman signal at 1580 cm^{-1} (G band), but also presents two emerging Raman bands at 1000–1200 cm^{-1} and 1300 cm^{-1} (D band). Herein, the appearance of D band indicates that some Ti atoms have been peeled away and



more C atoms are exposed to the surroundings [33]. Therefore, the integrated Raman intensity of FL-Ti₃C₂T_x in this range is slightly larger than that of ML-Ti₃C₂T_x, implying that FL-Ti₃C₂T_x adsorbs more terminal groups. Zeta potentials of ML-Ti₃C₂T_x and FL-Ti₃C₂T_x are -4.38 and -26.9 mV, respectively, as shown in Additional file 1: Fig. S1, which further confirm that FL-Ti₃C₂T_x are terminated by more groups with negative charges.

The UV-Vis spectra shown in Fig. 2b reveal that both FL-Ti₃C₂T_x and ML-Ti₃C₂T_x present two dominant absorption bands. In the UV region (225–325 nm), FL-Ti₃C₂T_x displays relatively stronger absorption band which corresponds to the band gap transition [34], implying that there are more -OH groups have been terminated on FL-Ti₃C₂T_x [35]. On the other hand, the comparison between the long wavelength absorption bands

(600–1000 nm) of both samples shows that the relative intensity of FL-Ti₃C₂T_x in this range is obviously lower than that of ML-Ti₃C₂T_x, indicating that ML-Ti₃C₂T_x are mainly terminated by $-O$ [35]. FL-Ti₃C₂T_x can be well dispersed in the aqueous solution since the terminated $-OH$ groups shows hydrophilicity and electrostatic repulsion between sheets [31, 36]. As for ML-Ti₃C₂T_x with more $-O$ terminals, it can only form a suspension in the beginning and will deposit subsequently as shown in Additional file 1: Fig. S2a.

In order to shed more light on the surface groups terminated on ML-Ti₃C₂T_x and FL-Ti₃C₂T_x, XPS spectra of both samples were collected and are shown in Fig. 3. All corresponding detailed information regarding the surface states are summarized in Additional file 1: Table S1. The fraction of Ti-C in FL-Ti₃C₂T_x (9.80%) is lower than

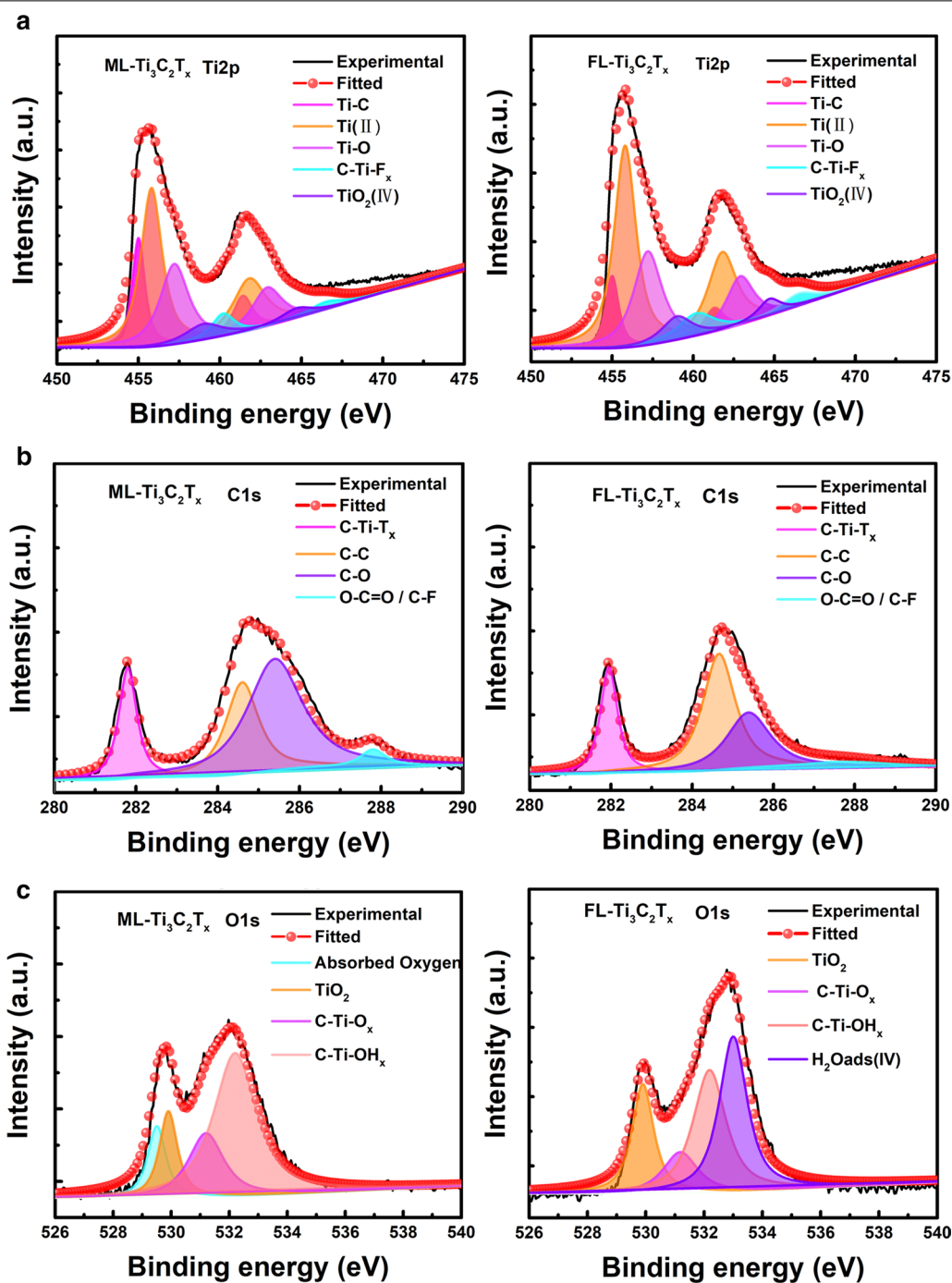


Fig. 3 XPS spectra of ML-Ti₃C₂T_x and FL-Ti₃C₂T_x **a** Ti2p, **b** C1s, **c** O1s

that in ML-Ti₃C₂T_x (17.31%), while the ratio of C–C in FL-Ti₃C₂T_x (44.62%) is higher. Such surface states changing evidences the loss of Ti atoms and the more exposed C atoms on the surface of FL-Ti₃C₂T_x, which agrees with the emerging D band in its Raman spectrum shown in Fig. 2a. The increased C-Ti-T_x ratio in FL-Ti₃C₂T_x

(21.27%) indicates that there should be more active terminal groups adsorbed on its surface than ML-Ti₃C₂T_x, which agrees with the Zeta potential results shown in Additional file 1: Fig. S1. Apart from the quantity of the terminal groups, the analysis of XPS results also reveals that FL-Ti₃C₂T_x and ML-Ti₃C₂T_x have been terminated

by different dominant functional groups, which also has been suggested by the (002) diffraction peaks shown in Fig. 1e. Regarding O 1s spectra of these two samples, it can be clearly seen that more O-related states have been found on the surface of ML-Ti₃C₂T_x, and some of them are adsorbed oxygen molecules, which can dissociate to form Ti₃C₂O_x and therefore will repel O₂ in air to prevent further oxidation of ML-Ti₃C₂T_x [37]. As a result, ML-Ti₃C₂T_x seems present a better oxidation resistance with a lower TiO₂ ratio (13.98%) than FL-Ti₃C₂T_x (19.60%).

Based on the observations and analyses of Figs. 1, 2 and 3, it can be concluded that although both ML-Ti₃C₂T_x and FL-Ti₃C₂T_x are terminated by some functional groups with negative charge, the amount and dominant type of the groups are quite different. On one hand, the quantity of terminal groups on FL-Ti₃C₂T_x is larger than that of ML-Ti₃C₂T_x. On the other hand, the dominant terminal structure on ML-Ti₃C₂T_x is Ti₃C₂O₂, which makes ML-Ti₃C₂T_x to be more stable in the air [38], while for FL-Ti₃C₂T_x, it is mainly terminated by Ti₃C₂(OH)₂, which helps FL-Ti₃C₂T_x to be well-dispersed in aqueous solutions [36].

Ti₃C₂T_x with functional terminal groups could reveal good adsorption performance and therefore could act as a surface-enhanced Raman scattering (SERS) substrate to improve the Raman activity of positively charged probe molecules [3, 39, 40]. Comparing with ML-Ti₃C₂T_x, FL-Ti₃C₂T_x should present better adsorption ability since it has been determined that it is terminated with more

negative charges. Such better adsorption performance has been demonstrated by the optical photographs of the mixed solution with R6G and FL-Ti₃C₂T_x as shown in Additional file 1: Fig. S2b. However, Fig. 4a reveals that the ML-Ti₃C₂T_x substrate obviously performs better SERS activity than FL-Ti₃C₂T_x one. Considering ML-Ti₃C₂T_x with -O terminal presents stronger absorption band centered at around 800 nm, which can be assigned to the surface plasmon resonant absorption [3, 15, 39, 41], it therefore can be concluded that ML-Ti₃C₂T_x with stronger SERS activity should result from the stronger near-field effect induced by the relatively stronger surface plasmon resonance as shown in Fig. 2b.

In order to further explore the relationship between the terminal groups and the near-field effect of Ti₃C₂T_x nanosheets, the hybrid structures composed of Ti₃C₂T_x nanosheets, including few layered and multilayered, and Ag nanoparticles (NPs) have been synthesized, which are accordingly labeled as Ag/FL-Ti₃C₂T_x and Ag/ML-Ti₃C₂T_x, respectively. The morphologies of both hybrid samples are shown in Additional file 1: Fig. S3. The insets indicate the corresponding size distributions of Ag NPs loading on ML-Ti₃C₂T_x (5–40 nm) is larger than that on FL-Ti₃C₂T_x (2–20 nm). Intuitively, it might be concluded that Ag/ML-Ti₃C₂T_x could perform better SERS activity than Ag/FL-Ti₃C₂T_x since both larger Ag NPs and relative stronger surface plasmon resonance of ML-Ti₃C₂T_x are beneficial to confine stronger near-field. However, the SERS spectra shown in Fig. 4b reveal a

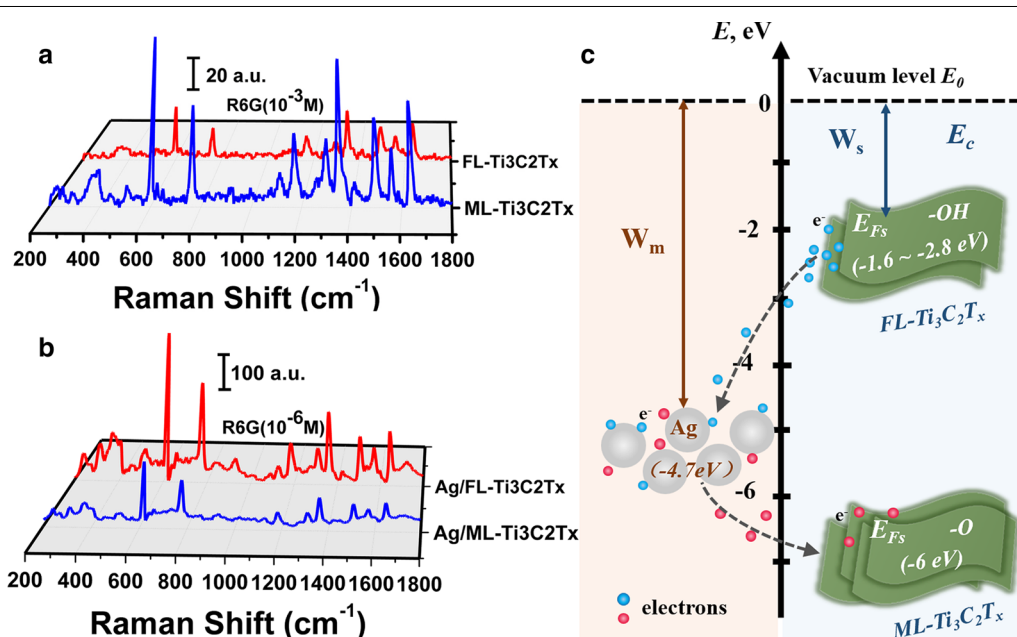


Fig. 4 **a** SERS spectra of R6G (10⁻³ M) with ML-Ti₃C₂T_x and FL-Ti₃C₂T_x. **b** SERS spectra of R6G (10⁻⁶ M) with Ag/ML-Ti₃C₂T_x and Ag/FL-Ti₃C₂T_x. **c** Schematic diagram of electron transfer from FL-Ti₃C₂T_x to Ag NP due to their work function difference. W_m and W_s represent the work functions of Ag NP and FL-Ti₃C₂T_x, respectively

counterintuitive result. It is clear that the enhancement effect offered by Ag/FL-Ti₃C₂T_x is nearly 3 times of that by Ag/ML-Ti₃C₂T_x, implying that the coupling between Ag NPs and FL-Ti₃C₂T_x should play an important role during the detection process. As confirmed above that FL-Ti₃C₂T_x has been mainly terminated by -OH groups with lots of surface electrons, which will result in the formation of Ti₃C₂(OH)₂ structure with a work function of 1.6–2.8 eV [42, 43]. As shown in Fig. 4c, the abundant surface electrons will therefore transfer from FL-Ti₃C₂T_x to Ag NPs with a work function of 4.7 eV [44]. With the extra injection of hot electrons from FL-Ti₃C₂T_x, Ag NPs with smaller size could present stronger resonance under the excitation and eventually perform better SERS activity due to the coupling induced stronger electromagnetic effect. It is worth noting that the work function of Ti₃C₂O₂ structure formed on the surface of ML-Ti₃C₂T_x is around 6.0 eV [43], which will result in electron transfer from Ag NPs surface to ML-Ti₃C₂T_x nanosheets and therefore will weaken the near-field enhanced effect supported by the Ag NPs. On the other hand, not like FL-Ti₃C₂T_x with -OH terminals, ML-Ti₃C₂T_x with -O terminals cannot offer sufficient electrons under excitation [42]. It is therefore reasonable that the SERS activity of Ag/ML-Ti₃C₂T_x is worse than that of Ag/FL-Ti₃C₂T_x.

Conclusions

In summary, ML-Ti₃C₂T_x and FL-Ti₃C₂T_x terminated with different dominant functional groups have been successfully prepared. It has been demonstrated that ML-Ti₃C₂T_x is more stable in the air due to the surface structure of Ti₃C₂O₂ and show stronger SERS activity than FL-Ti₃C₂T_x because it can reveal stronger near-field effect. However, FL-Ti₃C₂T_x terminated by Ti₃C₂(OH)₂ can be well dispersed in aqueous solution and will show better SERS performance after coupling to the Ag NPs due to the sufficient electron injection. Such research regarding the terminal groups-dependent near-field enhancement performance will help people to expand the potential applications of Ti₃C₂T_x in the optical related fields.

Abbreviations

ML-Ti₃C₂T_x: Multilayered Ti₃C₂T_x; FL-Ti₃C₂T_x: Few layered Ti₃C₂T_x; SERS: Surface enhanced Raman scattering; NPs: Nanoparticles.

Supplementary Information

The online version contains supplementary material available at <https://doi.org/10.1186/s11671-021-03510-5>.

Additional file 1. Figure S1. Zeta potentials of ML-Ti₃C₂T_x and FL-Ti₃C₂T_x. **Figure S2.** (a) Optical photographs of ML-Ti₃C₂T_x and FL-Ti₃C₂T_x. (b) Optical photographs of ML-Ti₃C₂T_x and FL-Ti₃C₂T_x soaking in R6G solutions. **Figure**

S3. TEM images of (a) Ag/ML-Ti₃C₂T_x and (b) Ag/FL-Ti₃C₂T_x. The insets are the size distributions of Ag NPs in the corresponding samples. **Table S1.** Surface states and corresponding relative contents extracted from the XPS Ti 2p, C 1s and O 1s spectra of ML-Ti₃C₂T_x and FL-Ti₃C₂T_x.

Acknowledgements

This work was financially supported by the National Natural Science Foundation of China (61675061 and 11774077), the Fundamental Research Funds for the Central Universities (PA2019GDQT0013), and the Provincial Innovation and Entrepreneurship Training Program for College Students (S201910359033).

Authors' contributions

YYY planned and conducted the experiment and wrote the manuscript. WTZ, WLS, QQZ, HJX, and YZ performed the background study and helped synthesis of nanosheets and hybrid samples. SC and PFL offered guidance on characterizations. YWL managed the checking and revising of the manuscript. All authors read and approved the final manuscript.

Funding

This work is supported by the National Natural Science Foundation of China (61675061 and 11774077), the Fundamental Research Funds for the Central Universities (PA2019GDQT0013), and the Provincial Innovation and Entrepreneurship Training Program for College Students (S201910359033).

Availability of data and materials

The raw dataset obtained analyzed during the experimental work is available from the corresponding author on reasonable request.

Declarations

Ethics approval and consent to participate

None.

Consent for publication

None.

Competing interests

The authors declare that they have no competing interests.

Author details

¹ School of Materials Science and Engineering, Hefei University of Technology, Hefei 230009, People's Republic of China. ² Instrumental Analysis Center, Hefei University of Technology, Hefei 230009, People's Republic of China. ³ Engineering Research Center of High Performance Copper Alloy Materials and Processing, Ministry of Education, Hefei University of Technology, Hefei 230009, People's Republic of China.

Received: 6 September 2020 Accepted: 21 March 2021

Published online: 12 April 2021

References

- Hong Ng VM, Huang H, Zhou K, Lee PS, Que W, Xu JZ, Kong LB (2017) Recent progress in layered transition metal carbides and/or nitrides (MXenes) and their composites: synthesis and applications. *J Mater Chem A* 5:3039–3068
- Cheng L, Li X, Zhang H, Xiang Q (2019) Two-dimensional transition metal MXene-based photocatalysts for solar fuel generation. *J Phys Chem Lett* 10:3488–3494
- Xiong D, Li X, Bai Z, Lu S (2018) Recent advances in layered Ti₃C₂T_x MXene for electrochemical energy storage. *Small* 14:1703419
- Yang J, Bao W, Jaumaux P, Zhang S, Wang C, Wang G (2019) MXene-based composites: synthesis and applications in rechargeable batteries and supercapacitors. *Adv Mater Interfaces* 6:1802004

5. Jiang X, Kuklin AV, Baev A, Ge Y, Ågren H, Zhang H, Prasad PN (2020) Two-dimensional MXenes: from morphological to optical, electric, and magnetic properties and applications. *Phys Rep* 848:1–58
6. Huang K, Li Z, Lin J, Han G, Huang P (2018) Two-dimensional transition metal carbides and nitrides (MXenes) for biomedical applications. *Chem Soc Rev* 47:5109–5124
7. Li T, Yao L, Liu Q, Gu J, Luo R, Li J, Yan X, Wang W, Liu P, Chen B et al (2018) Fluorine-free synthesis of high purity $Ti_3C_2T_x$ ($T = -OH, -O$) via alkali treatment. *Angew Chem Int Ed* 57:6115–6119
8. Li M, Lu J, Luo K, Li Y, Chang K, Chen K, Zhou J, Rosen J, Hultman L, Eklund P et al (2019) Element replacement approach by reaction with Lewis acidic molten salts to synthesize nanolaminated MAX phases and MXenes. *J Am Chem Soc* 141:4730–4737
9. Bian R, Lin R, Wang G, Lu G, Zhi W, Xiang S, Wang T, Clegg PS, Cai D, Huang W (2018) 3D assembly of Ti_3C_2 -MXene directed by water/oil interfaces. *Nanoscale* 10:3621–3625
10. Peng Q, Guo J, Zhang Q, Xiang J, Liu B, Zhou A, Liu R, Tian Y (2014) Unique lead adsorption behavior of activated hydroxyl group in two-dimensional titanium carbide. *J Am Chem Soc* 136:4113–4116
11. Enyashin AN, Ivanovskii AL (2013) Structural and electronic properties and stability of MXenes Ti_3C and Ti_3C_2 functionalized by methoxy groups. *J Phys Chem C* 117:13637–13643
12. Xie Y, Naguib M, Mochalin VN, Barsoum MW, Gogotsi Y, Yu X, Nam K-W, Yang X-Q, Kolesnikov AI, Kent PRC (2014) Role of surface structure on Li-ion energy storage capacity of two dimensional transition-metal carbides. *J Am Chem Soc* 136:6385–6394
13. Mauchamp V, Bugnet M, Bellido EP, Botton GA, Moreau P, Magne D, Naguib M, Cabioch T, Barsoum MW (2014) Enhanced and tunable surface plasmons in two-dimensional Ti_3C_2 stacks: electronic structure versus boundary effects. *Phys. Rev. B* 89: 235428
14. Jhon YI, Jhon YM, Lee JH (2020) Broadband ultrafast photonics of two-dimensional transition metal carbides (MXenes). *Nano Futures* 4:032003
15. Chaudhuri K, Alhabeib M, Wang Z, Shalae VM, Gogotsi Y, Boltasseva A (2018) Highly broadband absorber using plasmonic titanium carbide (MXene). *ACS Photonics* 5:1115–1122
16. Choi G, Shahzad F, Bahk Y-M, Jhon YM, Park H, Alhabeib M, Anasori B, Kim D-S, Koo CM, Gogotsi Y et al (2018) Enhanced Terahertz shielding of MXenes with nano-metamaterials. *Adv Opt Mater* 6:1701076
17. Velusamy DB, El-Demellawi JK, El-Zohry AM, Giugni A, Lopatin S, Hedhili MN, Mansour AE, Fabrizio ED, Mohammed OF, Alshareef HN (2019) MXenes for plasmonic photodetection. *Adv Mater* 31:1807658
18. Peng Y, Cai P, Yang L, Liu Y, Zhu L, Zhang Q, Liu J, Huang Z, Yang Y (2020) Theoretical and experimental studies of Ti_3C_2 MXene for surface-enhanced Raman spectroscopy-based sensing. *ACS Omega* 5:26486–26496
19. Yu M, Liu S, Su D, Jiang S, Zhang G, Qin Y, Li M-Y (2019) Controllable MXene nano-sheet/Au nanostructure architectures for the ultra-sensitive molecule Raman detection. *Nanoscale* 11:22230–22236
20. Benchakar M, Loupias L, Garnero C, Bilyk T, Morais C, Canaff C, Guignard N, Morisset S, Pazniak H, Hurand S et al (2020) One MAX phase, different MXenes: a guideline to understand the crucial role of etching conditions on $Ti_3C_2T_x$ surface chemistry. *Appl Surf Sci* 530:147209
21. Ding S-Y, You E-M, Tian Z-Q, Moskovits M (2017) Electromagnetic theories of surface-enhanced Raman spectroscopy. *Chem Soc Rev* 46:4042–4076
22. Hantanasirisakul K, Gogotsi Y (2018) Electronic and optical properties of 2D transition metal carbides and nitrides (MXenes). *Adv Mater* 30:1804779
23. Fan X, Ding Y, Liu Y, Liang J, Chen Y (2019) Plasmonic $Ti_3C_2T_x$ MXene enables highly efficient photothermal conversion for healable and transparent wearable device. *ACS Nano* 13:8124–8134
24. Peng Y, Lin C, Long L, Masaki T, Tang M, Yang L, Liu J, Huang Z, Li Z, Luo X et al (2021) Charge-transfer resonance and electromagnetic enhancement synergistically enabling MXenes with excellent SERS sensitivity for SARS-CoV-2 S protein detection. *Nano-Micro Lett* 13:52
25. Hope MA, Forse AC, Griffith KJ, Lukatskaya MR, Ghidui M, Gogotsi Y, Grey CP (2016) NMR reveals the surface functionalisation of Ti_3C_2 MXene. *Phys Chem Chem Phys* 18:5099–5102
26. Ghidui M, Lukatskaya MR, Zhao M-Q, Gogotsi Y, Barsoum MW (2014) Conductive two-dimensional titanium carbide 'clay' with high volumetric capacitance. *Nature* 516:78–81
27. Peng C, Wang C-A, Song Y, Huang Y (2006) A novel simple method to stably synthesize Ti_3AlC_3 powder with high purity. *Mater Sci Eng A* 428:54–58
28. Mashtalir O, Naguib M, Mochalin VN, Dall'Agnese Y, Heon M, Barsoum MW, Gogotsi Y (2013) Intercalation and delamination of layered carbides and carbonitrides. *Nat Commun* 4:1–7
29. Xuan J, Wang Z, Chen Y, Liang D, Cheng L, Yang X, Liu Z, Ma R, Sasaki T, Geng F (2016) Organic-base-driven intercalation and delamination for the production of functionalized titanium carbide nanosheets with superior photothermal therapeutic performance. *Angew Chem Int Ed* 55:14569–14574
30. Naguib M, Kurtoglu M, Presser V, Lu J, Niu J, Heon M, Hultman L, Gogotsi Y, Barsoum MW (2011) Two-dimensional nanocrystals produced by exfoliation of Ti_3AlC_3 . *Adv Mater* 23:4248–4253
31. Yan J, Ren CE, Maleski K, Hatter CB, Anasori B, Urbankowski P, Sarycheva A, Gogotsi Y (2017) Flexible MXene/graphene films for ultrafast supercapacitors with outstanding volumetric capacitance. *Adv Funct Mater* 27:1701264
32. Hu T, Wang J, Zhang H, Li Z, Hu M, Wang X (2015) Vibrational properties of Ti_3C_2 and $Ti_3C_2T_2$ ($T = O, F, OH$) monosheets by first-principles calculations: a comparative study. *Phys Chem Chem Phys* 17:9997–10003
33. Tong Y, He M, Zhou Y, Zhong X, Fan L, Huang T, Liao Q, Wang Y (2018) Electromagnetic wave absorption properties in the centimetre-band of $Ti_3C_2T_x$ MXenes with diverse etching time. *J Mater Sci-Mater El* 29:8078–8088
34. Satheeshkumar E, Makaryan T, Melikyan A, Minassian H, Gogotsi Y, Yoshimura M (2016) One-step solution processing of Ag, Au and Pd@MXene hybrids for SERS. *Sci Rep* 6:32049
35. Berdiyrov GR (2016) Optical properties of functionalized $Ti_3C_2T_2$ ($T = F, O, OH$) MXene: first-principles calculations. *AlP Adv* 6:055105
36. Lukatskaya MR, Mashtalir O, Ren CE, Dall'Agnese Y, Rozier P, Taberna PL, Naguib M, Simon P, Barsoum MW, Gogotsi Y (2013) Cation intercalation and high volumetric capacitance of two-dimensional titanium carbide. *Science* 341:1502–1505
37. Gan L-Y, Huang D, Schwingenschlögl U (2013) Oxygen adsorption and dissociation during the oxidation of monolayer Ti_2C . *J Mater Chem A* 1:13672–13678
38. Fu ZH, Zhang QF, Legut D, Si C, Germann TC, Lookman T, Du SY, Francisco JS, Zhang RF (2016) Stabilization and strengthening effects of functional groups in two-dimensional titanium carbide. *Phys Rev B* 94:104103
39. Sarycheva A, Makaryan T, Maleski K, Satheeshkumar E, Melikyan A, Minassian H, Yoshimura M, Gogotsi Y (2017) Two-dimensional titanium carbide (MXene) as surface-enhanced Raman scattering substrate. *J Phys Chem C* 121:19983–19988
40. Guo J, Peng Q, Fu H, Zou G, Zhang Q (2015) Heavy-metal adsorption behavior of two-dimensional alkalization intercalated MXene by first-principles calculations. *J Phys Chem C* 119:20923–20930
41. Lin H, Wang X, Yu L, Chen Y, Shi J (2017) Two-dimensional ultrathin MXene ceramic nanosheets for photothermal conversion. *Nano Lett* 17:384–391
42. Khazaei M, Ranjbar A, Ghorbani-Asl M, Arai M, Sasaki T, Liang Y, Yunoki S (2016) Nearly free electron states in MXenes. *Phys Rev B* 93:205125
43. Chertopalov S, Mochalin VN (2018) Environment-sensitive photoresponse of spontaneously partially oxidized Ti_3C_2 MXene thin films. *ACS Nano* 12:6109–6116
44. Lu Y-W, Hu Y, Huang C, Cheng S, Xu C-X, Luo P-F, Cheng J-G, Jang Y (2016) Enhanced plasmon radiative intensity from Ag nanoparticles coupled to a graphene sheet. *Appl Phys Lett* 108:153113

Publisher's Note

Springer Nature remains neutral with regard to jurisdictional claims in published maps and institutional affiliations.